

# Eco-Friendly Corrosion Inhibition of AA2024 in 3.5% NaCl Using the Extract of *Linum usitatissimum* Seeds

Hassan Elgahawi<sup>1,3</sup> · Mohamed Gobara<sup>2</sup>  · Ahmad Baraka<sup>2</sup> · Waleed Elthalabawy<sup>3</sup>

Received: 31 July 2017 / Revised: 16 October 2017 / Accepted: 21 October 2017 / Published online: 26 October 2017  
© Springer International Publishing AG 2017

**Abstract** Inhibitive effect of the extract of *Linum usitatissimum* seeds (*ELUS*) on the corrosion of the aluminum alloy AA2024 immersed in NaCl solution (3.5%) was studied by potentiodynamic polarization (PDP), electrochemical impedance spectroscopy (EIS) and electrochemical noise measurement (EN) techniques. *ELUS* effectively inhibited the corrosion of AA2024 with efficiency ranges from 65 to 82% for the corresponding *ELUS* concentrations from 80 to 1200 ppm. PDP showed that *ELUS* works as a cathodic inhibitor for aluminum in 3.5% NaCl solution. EIS showed that the corrosion process was governed by the charge transfer resistance ( $R_{ct}$ ), where  $R_{ct}$  values gradually increase with the increase in *LU* concentration. The results of EN are in a good agreement with the PDP and EIS results. Also, SEM confirms the electrochemical results.

**Keywords** Corrosion · GC–MS · EN · EIS

## 1 Introduction

Generally, all industrial metals suffer from corrosion. It does not only cost the economy 3–4% of gross national product [1] but also affect human health and safety. It has a rising effect from overdesign to maintenance to the failure of equipment and finally causes a shutdown.

Aluminum alloys have been extensively used in many industries such as cars, pipes, construction, batteries and aircraft. Aluminum alloy 2024-T3 is well known in aerospace applications due to its high strength to weight ratio and good fatigue resistance [2]. However, the inhomogeneous distribution of intermetallic particles within the aluminum matrix generates local galvanic cells that affect the corrosion resistance.

Compact, adherent and continuous oxide film is developed on aluminum upon exposure to the atmosphere or aqueous solutions. This film is responsible for the corrosion resistance in a dry atmosphere. However, it cannot protect aluminum exposed to severe environments. Moreover, aluminum may be used in neutral solutions containing pitting agents such as chloride ions. Hence, anti-corrosion measures should be applied. One of these measures is the use of inhibitors, which is an efficient method for metal protection. Numerous researches have been conducted to present effective inhibitors suitable for different corrosive media [3–8]. Some of these inhibitors have negative impact on the environment such as chromates [9]. A considerable number of inorganic inhibitors have good metal protection performance with low toxicity; however, most of these inhibitors are expensive [3]. Green chemistry, economics and waste treatment all favor the use of environmental-friendly inhibitors such as organic corrosion inhibitors (especially those from natural sources), which became, nowadays, of practical interest. Metal protection by these organic inhibitors comes from the fact that they adsorb on the metal surface forming a protective layer against corrosive species in the media [10]. The efficiency of an inhibitor depends on many factors such as the nature of the metal surface, the type of corrosive media and the chemical structure of the inhibitor. The chemical structure of the organic inhibitor and its charge density are crucial since they dictate the mode of adsorption

---

✉ Mohamed Gobara  
m\_gobara@yahoo.com

<sup>1</sup> Libyan Armed Force, Tripoli, Libya

<sup>2</sup> Chemical Engineering Department, Military Technical College, Cairo Governorate, Egypt

<sup>3</sup> Metallurgy Engineering Department, Military Technical College, Cairo Governorate, Egypt

on the metal surface and the number of metal-surface-active centers that could be covered [4, 11].

*Linum usitatissimum* is one of the oldest known cultivated plants, and it was found in ancient Egyptian tombs. It has been used in textile and paper industries. Edible oil is extracted by pressing the *L. usitatissimum* seeds where the rest (solid residues) can be used for feeding cattle.

This study aimed to investigate the inhibition efficiency of the extract of *Linum Usitatissimum* seeds (*ELUS*) on the corrosion of AA2024 in NaCl solution (3.5%) as a corrosive media. Three electrochemical applications were applied for the investigation: potentiodynamic polarization (PDP), electrochemical impedance spectroscopy (EIS) and electrochemical noise (NE) measurements. IR, chromatography analyses, optical imaging, SEM and EDX mapping were applied to give more understandings for inhibition behavior.

## 2 Experimental Work

### 2.1 Specimen Preparation

A sheet of aluminum alloy (AA2024, composition in wt%: Mn(1.28), pb(0.064), Zn(0.006), Ti(0.029), Cu(0.81), Si(0.381), Fe(0.57) and Al(96.65%)), was obtained from Q-panel™. The sheet was pressed-cut into coupons each with dimensions 2.0 cm × 5.0 cm × 0.1 cm. Coupons were degreased and cleaned with ethanol and allowed to dry and then stored in a desiccator until their use in corrosion experiments [5]. The corrosive solution (3.5% aqueous NaCl, Sigma-Aldrich) and all other solutions were prepared using deionized water.

### 2.2 Preparation of Inhibitor

The seeds of *L. Usitatissimum* were purchased from a local market, Cairo, Egypt. For extraction, 50 g of the seeds was washed with deionized water and then was soaked in water/ethanol solution in a closed vial (v/v = 80:20, 200 ml), which was kept in an oven at 90 °C for 4 h. The vial was then removed from the oven and was left to cool to the room temperature. The produced solution was filtrated, and the filtrate was dried by heating (50 °C) under vacuum for 24 h. The produced dry extract powder of the *ELUS* inhibitor was then collected, weighed and stored at 4 °C until the use. For each corrosion experiment, without any further purification or processing, a specified amount of *ELUS* was directly added to the corrosive medium.

### 2.3 Characterization Studies

The Agilent 5975T LTM GC/MSD with a stationary phase DB-5H30mx with 0.319 mm × 0.10 μm of phase thickness

was used to analyze the *ELUS*. *ELUS* powder was dissolved in 1, 2 dichloroethane solvent forming the analyte solution. Helium was used as the carrier gas, and a sample of analyte solution (1 μl) was injected into the column at an initial temperature of 50 °C. Heating was programmed to increase the temperature up to 150 °C at 5 °C/min rate. The temperature of the mass detector was 250 °C where the MS detector was operated. The mass spectrum of the sample was compared with the internal standard mass spectrum (Mass Spectral Database NIST/EPA/NIH) to define the unknown components. Based on the total area values of the identified peaks, the percentage of each component was determined by the relative area of each peak.

To determine the functional groups of the inhibitor, a dry certain amount of *ELUS* was thoroughly mixed with KBr powder and then pressed to form a transparent disk. The IR spectrum of this disk was recorded in the range of 400–4000 cm<sup>-1</sup> with an automatic signal gain that collected by 500 scans at 4 cm<sup>-1</sup> resolution using the FTIR spectrometer (JASCO Model 4100, Japan). The background spectrum was recorded from the clean empty cell at 25 °C and was taken into consideration during analysis of the *ELUS* sample.

The surface morphology of the coated metal samples was investigated using scanning electron microscope (SEM, Carl Zeiss EVO-10) equipped with an energy-dispersive X-ray spectroscopy (EDS) analyzer.

### 2.4 Electrochemical Characterization Studies

Potentiostat/galvanostat with three-electrode type cell was used for electrochemical corrosion experiments using Gamry™, model reference 600. For all experiments, the ratio of corrosive solution volume to sample surface area is not less than 40 ml/cm<sup>2</sup>.

For each experiment, a freshly prepared AA2024 coupon was used as working electrode, saturated calomel electrode as a reference electrode and platinum as the auxiliary electrode. The potentiodynamic polarization experiments were performed after immersion of the working electrode for at least 30 min in the corrosive solution. The potentiodynamic polarization curves were obtained in the potential ranges of – 250 to – 250 mV with respect to open-circuit potential (*OCP*) at a scan rate of 0.5 mV/s.

The EIS tests were performed at room temperature by a three-electrode assembly. A saturated calomel electrode was used as a reference electrode, platinum as a counter electrode and freshly prepared AA2024 as the working electrode. The EIS tests were performed using a Gamry reference 600 instrument in a frequency range of 10<sup>5</sup>–10<sup>-2</sup> Hz with an amplitude of 10 mV peak to peak, using AC signal at *OCP*. Inhibition efficiency ( $\eta$ ) is calculated using [12]:

$$\eta = \frac{(R_{ct} - R_{ct}^o)}{R_{ct}} \times 100$$

where  $R_{ct}^o$  and  $R_{ct}$  ( $\Omega \text{ cm}^2$ ) are the charge transfer resistance in the absence and in the presence of inhibitor, respectively.

The electrochemical noise technique was also used in this study. The electrochemical potential ( $V_{i \text{ noise}}$ ) and current ( $I_{i \text{ noise}}$ ) noises were simultaneously determined in a freely corroding system employing two nominally identical working electrodes of the same area ( $2.0 \text{ cm} \times 5.0 \text{ cm} \times 0.1 \text{ cm}$ ), and a saturated calomel reference electrode was placed in middle distance between the two working electrodes. The noise data were recorded for 1800 s at a sampling frequency of 1 Hz. All data analysis was performed using EAS410 Gamry software.

### 3 Results and Discussion

#### 3.1 Inhibitor Characterization

*ELUS* was analyzed by GC/MS, and the resulting chromatogram is given in Fig. 1. The retention times of the most intense peaks with the corresponding suggested compounds are presented in Table 1. These are organic compounds and constitute 97.1% of the extract. The mass spectra of these compounds (not shown) indicate their chemical structures where most of them are fatty acids.

The FTIR spectrum of *ELUS* is presented in Fig. 2. The spectrum indicates the groups of the above compounds collectively. The broad peak at  $3429.8 \text{ cm}^{-1}$  can be assigned to O–H stretching.  $\text{CH}_2$  and  $\text{CH}_3$  stretching appear at  $2855$  and  $2930 \text{ cm}^{-1}$ , respectively [13]. The peak at  $1631.8 \text{ cm}^{-1}$  may be attributed to the stretching mode of C=O group, and peak at  $1388 \text{ cm}^{-1}$  represents the deformation of  $\text{CH}_2$  and/or  $\text{CH}_3$

**Table 1** Composition of *ELUS*

Compound	Molecular formula	Retention time (min)	Content%
Cetylic acid	$\text{C}_{18} \text{H}_{30} \text{O}_2$	7.7	4.3
Palmitic acid	$\text{C}_{16} \text{H}_{32} \text{O}_2$	8.9	7.8
Methyl linoleate	$\text{C}_{19} \text{H}_{32} \text{O}_2$	9.2	3.1
Linoleic acid	$\text{C}_{18} \text{H}_{32} \text{O}_2$	9.5	3.5
Linolenic acid	$\text{C}_{18} \text{H}_{30} \text{O}_2$	10.5	14.3
Oleic acid amid	$\text{C}_{18} \text{H}_{35} \text{ON}$	10.7	8.1
Stearic acid	$\text{C}_{18} \text{H}_{36} \text{O}_2$	12.4	56.1

[14]. The peak at 1351.1 represents the C–H bending. Also, a peak at 1117.5 should correspond to C–O stretch. The peak at 1597.5 is attributed to N–H of the amino group [15]. The peak at 2954.6 is related to the amide group. Almost all of these groups are well-known constituents of the fatty acids indicated by GC/MS analysis.

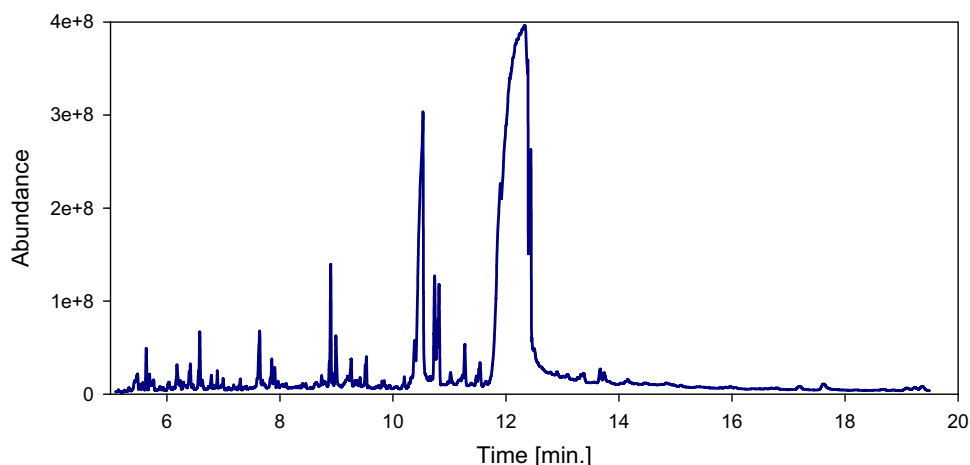
#### 3.2 Corrosion Measurements of Aluminum in 3.5% NaCl

The inhibition effect of *ELUS* on the aluminum corrosion in 3.5% NaCl solution was investigated by potentiodynamic polarization, electrochemical impedance spectroscopy and electrochemical noise (EN) techniques as given below.

##### 3.2.1 Potentiodynamic Polarization (PDP)

Anodic and cathodic polarization curves of AA2024 immersed in 3.5% NaCl solutions, in the absence and presence of different concentrations of *ELUS*, are shown in Fig. 3. It can be seen in the figure that the increase

**Fig. 1** Chromatogram of *ELUS*



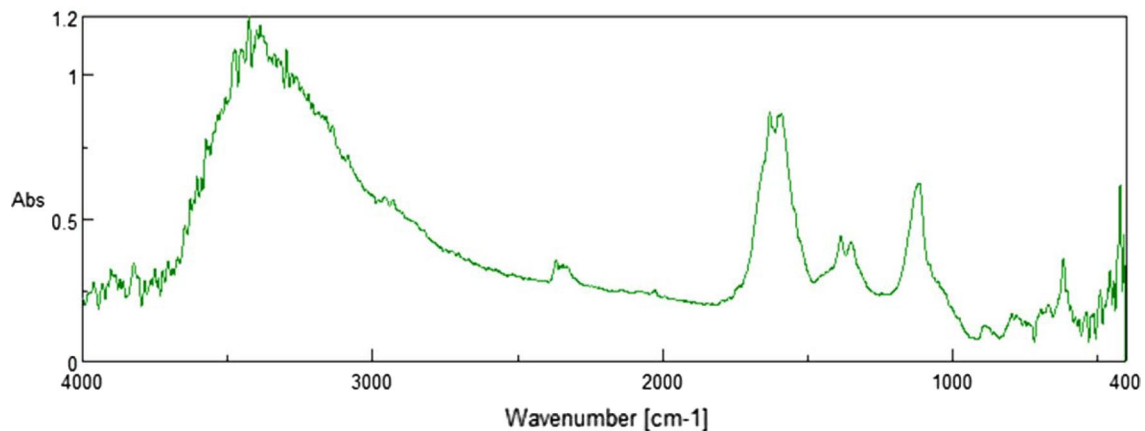


**Fig. 2** FTIR spectra of LU powder

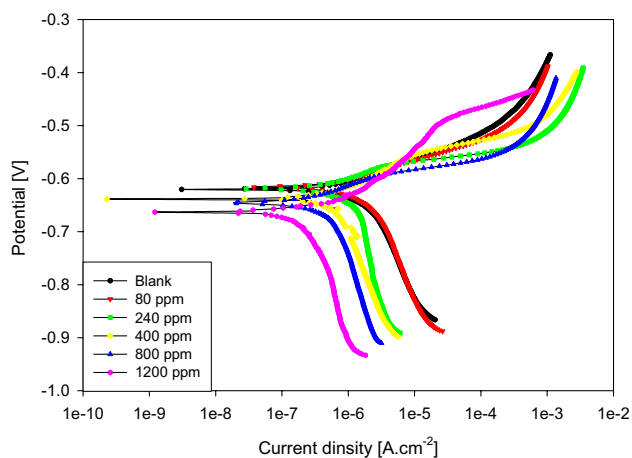


**Fig. 3** Tafel plots of aluminum in 3.5% NaCl with different concentrations of ELUS inhibitor at room temperature

in *ELUS* concentration caused more negative corrosion potentials. The cathodic branches shifted, with respect to that of the blank sample, to the lower current density region, which resulted in a significant decrease in  $I_{\text{corr}}$ . On the other hand, the anodic current densities did not considerably affect by the presence of *ELUS* when compared to the blank solution. This phenomenon clearly indicates

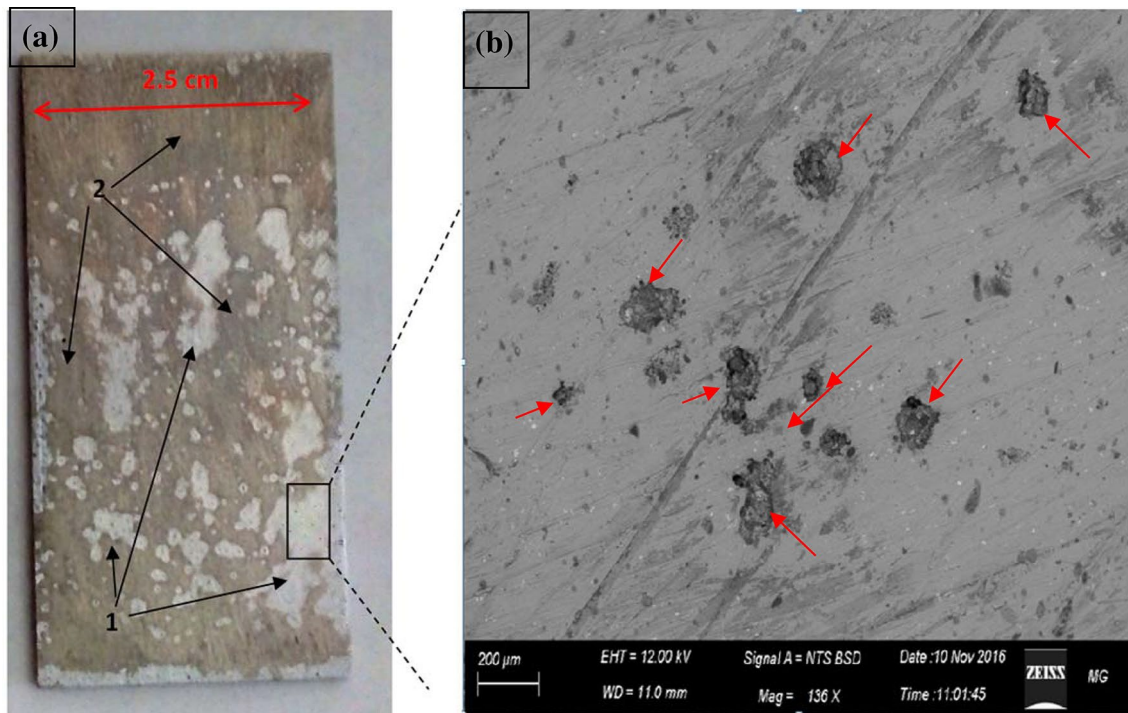
that *ELUS* acts as a cathodic inhibitor for aluminum in 3.5% NaCl solution [16–18].

Table 2 summarizes the electrochemical kinetic parameters of Tafel extrapolations ( $E_{\text{corr}}$ ,  $\beta_c$ ,  $\beta_a$ ,  $I_{\text{corr}}$ ,  $IE\%$ ). We note from the table that the increase in *ELUS* concentration results in a considerable regular decrease in corrosion current density ( $I_{\text{corr}}$ ) and a regular increase in inhibition efficiency ( $IE\%$ ) where inhibition efficiency of 82% was achieved by using 1200 ppm of *ELUS*.

For the concentration 80 ppm of inhibitor, from the table the recorded corrosion current density is higher than that of the blank sample (0 ppm) and it is worthy to comment on that behavior. There is always a threshold inhibitor concentration (minimum effective concentration) above which inhibition starts to perform in a regular manner with concentration [19]. Below this concentration, on the contrary, a serious corrosion could occur because the amount of inhibitor is not adequate to cover the whole surface of the metal surface, resulting in the build-up of two areas: the inhibitor-covered area and the bare area. Under this circumstance, the bare area behaves as an anode with respect to the cathodic reaction (reduction of oxygen). When the cathodic has a greater area than the anodic area (which called “unfavorable area ratio”), the corrosion process accelerates rather than being inhibited [20]. This phenomenon can be confirmed by observing the optical image of the corresponding sample

**Table 2** Corrosion kinetic parameters of aluminum with different concentrations of *ELUS* inhibitor

Conc. (ppm)	$\beta_a$ (mV/decade)	$\beta_c$ (mV/decade)	$E_{\text{corr}}$ (mV)	$I_{\text{corr}}$ (mA cm <sup>-2</sup> )	$IE\%$
0	0.084	0.275	– 621	44.7	–
80	0.077	0.318	– 615	52.1	–
240	0.060	0.469	– 619	16.90	65%
400	0.062	0.302	– 639	15.10	67%
800	0.060	0.348	– 645	10.00	78%
1200	0.083	0.556	– 663	8.16	82%



**Fig. 4** Images of AA 2024 immersed in 80 ppm ELUS: **a** optical image and **b** SEM magnification of selected area

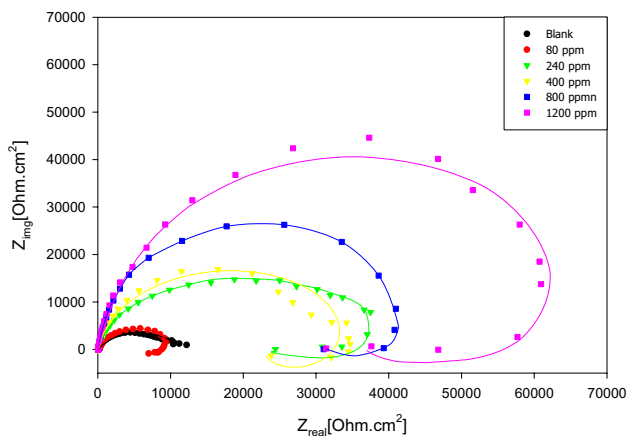


**Fig. 5** Nyquist plots AA2024 in 3.5% NaCl solution with different *ELUS* concentrations at room temperature

surface (Fig. 4a) where the two areas can be easily distinguished (arrows 1 and 2). For arrow 1, the surface is bright metallic and shows numerous pits. For arrow 2, on the other hand, the surface is dark, indicating that the surface is covered with the inhibitor and no pitting was optically observed. By investigating the bright metallic area using SEM imaging, Fig. 4b clearly shows the pits (red arrows). These observations are in consistent with that 80 ppm is less than the threshold concentration of inhibitor.

### 3.3 Electrochemical Impedance Spectroscopy (EIS)

Nyquist plots of AA2024 in 3.5% NaCl in the absence and in the presence of various concentrations of *ELUS* are shown in Fig. 5. The most marked observation to emerge from the figure is that all the plots are semicircles (in the absence and in the presence of the inhibitor). From the figure, the diameter of the capacitive loop increases, i.e., the impedance of the inhibited substrate increases, with the increase in the inhibitor concentration. Sample with 80 ppm shows exception which concurs well with the PDP results.

The impedance plots have a capacitive loop that covers the whole range of frequency under uninhibited condition. Under inhibited condition, the Nyquist plot consists of a larger capacitive loop at high frequencies and an inductive loop at low frequencies. The appearance of the inductive loop at low-frequency range, with inhibitor, suggests the adsorption of inhibitor molecule [21–23]. The capacitive loop at high frequency is related both to the charge transfer resistance of the corrosion process and to the double-layer capacitance.

The Bodes plots (impedance and phase in Figs. 6, 7) confirm the Nyquist plot results where the impedance increases as the *ELUS* concentration increases. Also, the phase plot reveals a single time constant, which increases with the increase in *ELUS* concentration [24]. Besides, the inductive loop was presents in the impedance plot, in Fig. 6, as a decrease in impedance at low-frequency range.



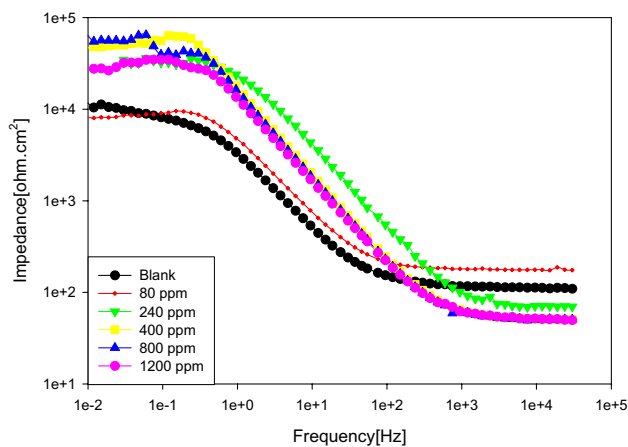


**Fig. 6** Impedance plots of AA2024 in 3.5% NaCl solution with different ELUS concentrations at room temperature

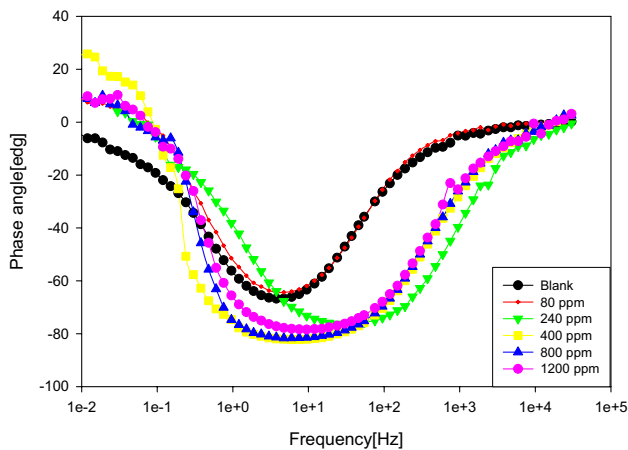


**Fig. 7** Phase angle plots of AA2024 in 3.5% NaCl solution with different ELUS concentrations at room temperature

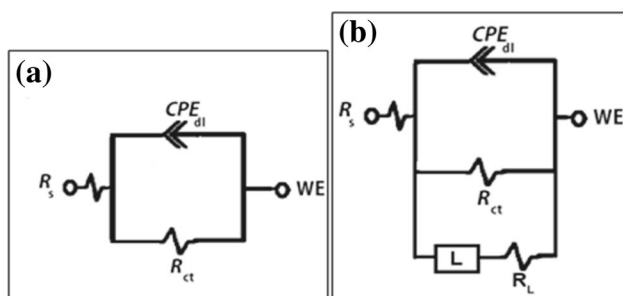


**Fig. 8** Equivalent circuits used for numerical fitting of the EIS data (a) in the absence and (b) in the presence of ELUS

In an attempt to understand the corrosion behavior of the ELUS inhibitor, EIS data were fitted to equivalent circuits, as shown in Fig. 8, where  $R_s$  is the solution resistance,  $R_{ct}$  is the charge transfer resistance,  $C_{dl}$  is the double-layer capacitance

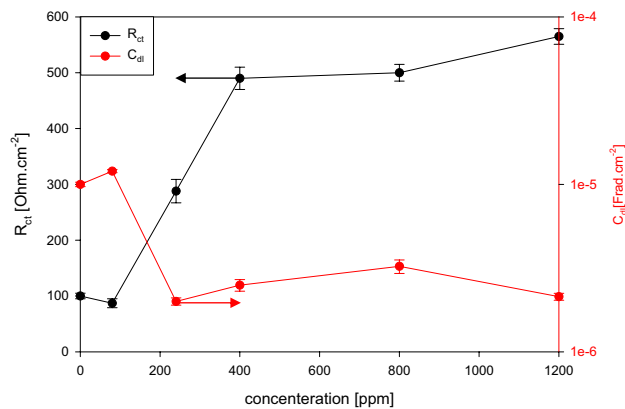


**Fig. 9** Changes in charge transfer resistance and double-layer capacitance of aluminum in 3.5% NaCl solution with a different concentration of ELUS at room temperature

and  $L$  is an inductive element. In this study, a leaking capacitor, constant phase element (CPE), is used instead of the pure capacitor for double-layer capacitance. The capacitance value can be calculated according to the following equation:

$$C_{dl} = \frac{Y_0 \omega^{n-1}}{\sin(n\pi/2)} \tag{1}$$

where  $Y_0$  is the CPE constant,  $\omega$  is the angular frequency (rad/s) and  $n$  is the CPE exponent. The CPE becomes pure capacitor when  $n = 1$ .

The change of both charge transfer resistance and double-layer capacitance of AA2024 in 3.5% NaCl solutions with a different concentration of ELUS is demonstrated in Fig. 9. From the figure,  $R_{ct}$  generally displays a significant increase with the increase in ELUS concentration, while  $C_{dl}$  shows an insignificant decrease. It is important to note that the corrosion inhibition of AA2024 depends mainly on the charge transfer resistance rather than the double-layer capacitance, which may be related to the adsorbed ELUS molecules on the aluminum surface (Table 3).

### 3.4 Electrochemical Noise (NE) Measurement

Electrochemical noise technique has many advantages such as its capability to differentiate between the different types of corrosion (uniform, crevice, and pitting), and it is applied without any external effect to the corroded sample [25, 26]. The main corrosion type of AA2024 in chloride containing solutions is the pitting; therefore, it was decided to use NE in this study. The noise resistance ( $R_n$ ) is determined in the time domain as the ratio of the standard deviation of potential noise ( $\sigma_V$ ) to that of current noise ( $\sigma_I$ ) is given by the following equation:

$$R_n = \frac{\sigma_V}{\sigma_I} \tag{2}$$

**Table 3** EIS fitting parameters with ELUS concentrations

ELUS (ppm)	$R_s$ ( $\Omega \text{ cm}^2$ )	$R_{ct}$ ( $\Omega \text{ cm}^2$ )	$Y_o$ ( $10^{-4} \times \text{Frad.cm}^{-2}$ )	$n$	$C_{dl}$ ( $10^{-5} \times \text{Frad.cm}^{-2}$ )	IE%
0	113.0	103	0.73	0.81	1.04	–
80	177.9	68	0.36	0.88	3.15	–
240	69.20	290	0.15	0.91	0.21	64.4%
400	52.94	489	0.094	0.95	0.24	78.9%
800	52.58	499	0.098	0.96	0.32	79.3%
1200	53.58	558	0.117	0.94	0.21	81.5%

where

$$\sigma_v = \sqrt{\frac{\sum_{i=1}^n (V_i - m_v)^2}{n}} \quad m_v = \frac{\sum_{i=1}^n V_i}{n} \quad (3)$$

$$\sigma_I = \sqrt{\frac{\sum_{i=1}^n (I_i - m_I)^2}{n}} \quad \text{and} \quad m_I = \frac{\sum_{i=1}^n I_i}{n} \quad (4)$$

The tendency of DC was detached before the analysis of noise data in time domain. It is claimed that DC trend

can cause inaccuracy in the calculation of noise resistance from time-domain analysis [27, 28]. Among different trend removal methods, the moving average removal (MAR) method was used in this study [29, 30]. The main feature of MAR method is a de-trending by subtracting a local average from the raw noise data. Any data point in the series,  $V_i$ , is a combination of the real noise component and the DC trend component:

$$V_i = V_{i,\text{noise}} + V_{i,\text{DC}} \quad (5)$$

$V_{i,\text{noise}}$  is the real noise, and it is required for noise resistance calculation where  $V_{i,\text{DC}}$  is the DC trend component,

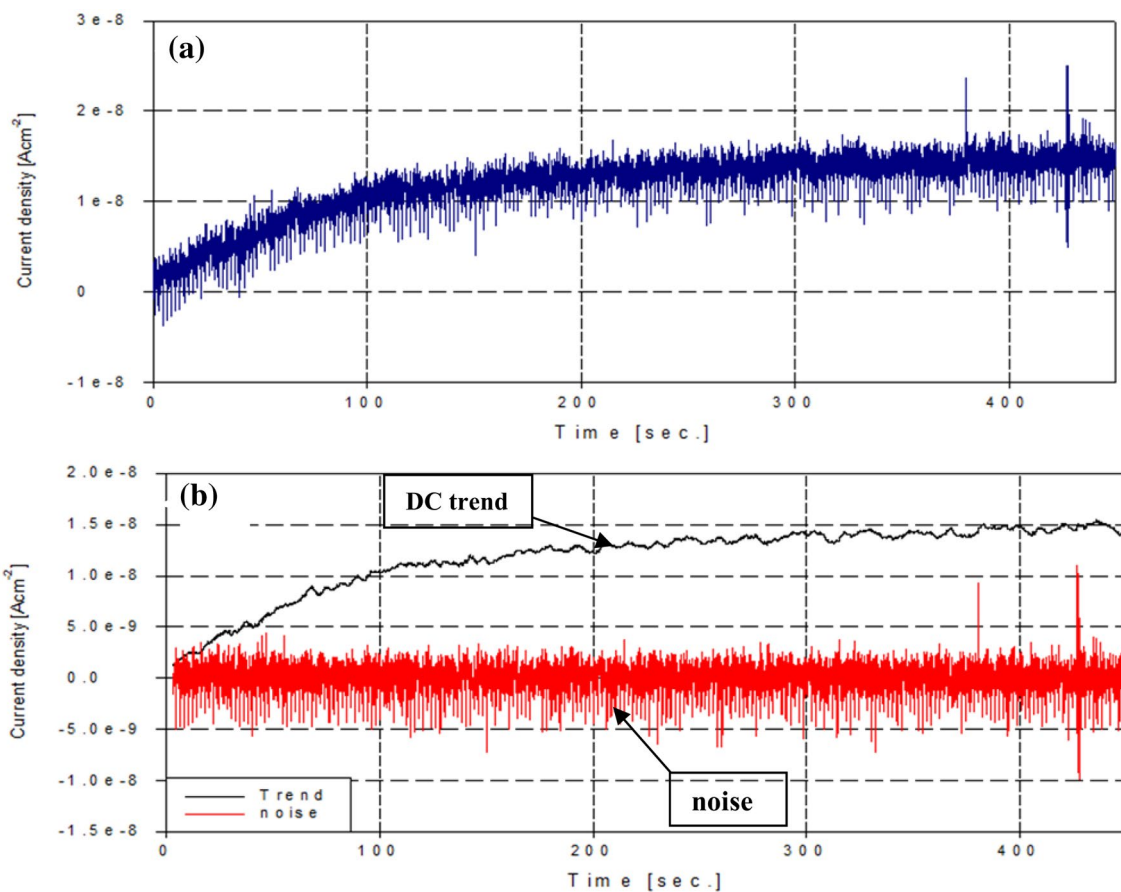


**Fig. 10** Time records of electrochemical current noise associated with AA2024 exposed to 3.5% NaCl solution with 240 ppm of ELUS at room temperature: (a) before and (b) after removal of DC trend (MAR parameter  $p = 64$ )

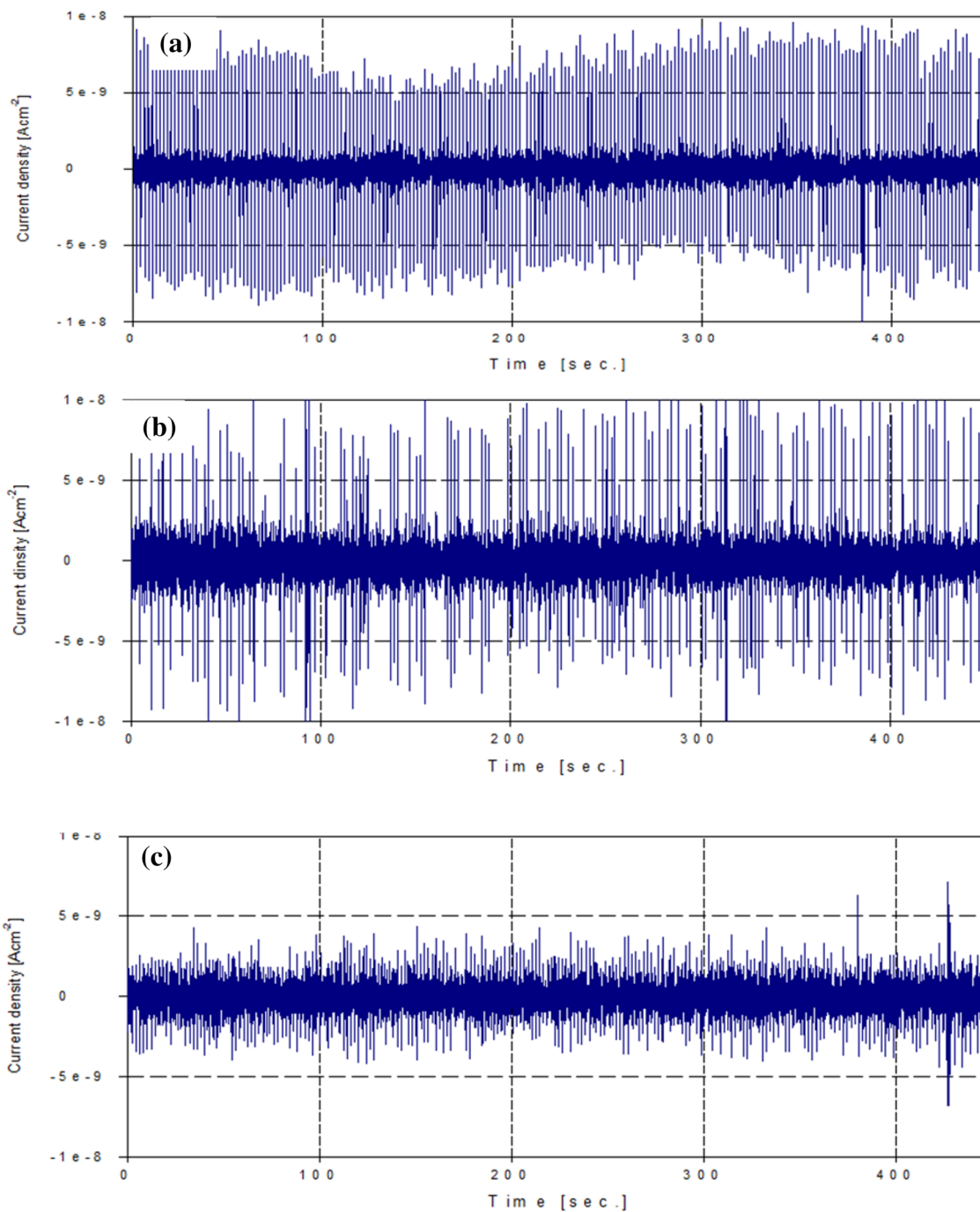


**Fig. 11** Time records of electrochemical current noise associated with AA2024 exposed to 3.5% NaCl solution with: **a** 0, **b** 80, **c** 240, **d** 400, **e** 800 and **f** 1200 ppm of *ELUS* inhibitor at room temperature

which has to be removed. The  $V_{i,DC}$  values can be calculated according to the following equation:

$$V_{i,DC} = \frac{\sum_{i-p}^{i+p+1} V_i}{2p + 2} \tag{6}$$

where  $p$  is an integer value that can be 3, 10, 16, 32, 50 or 64 [27, 28]. In this study,  $p$  values were taken = 64 to avoid over-filter of long lifetime electrochemical events [28]. The DC trend in the voltage–time record can, therefore, be removed, and the random fluctuation  $V_{i,noise}$  can be deduced as:



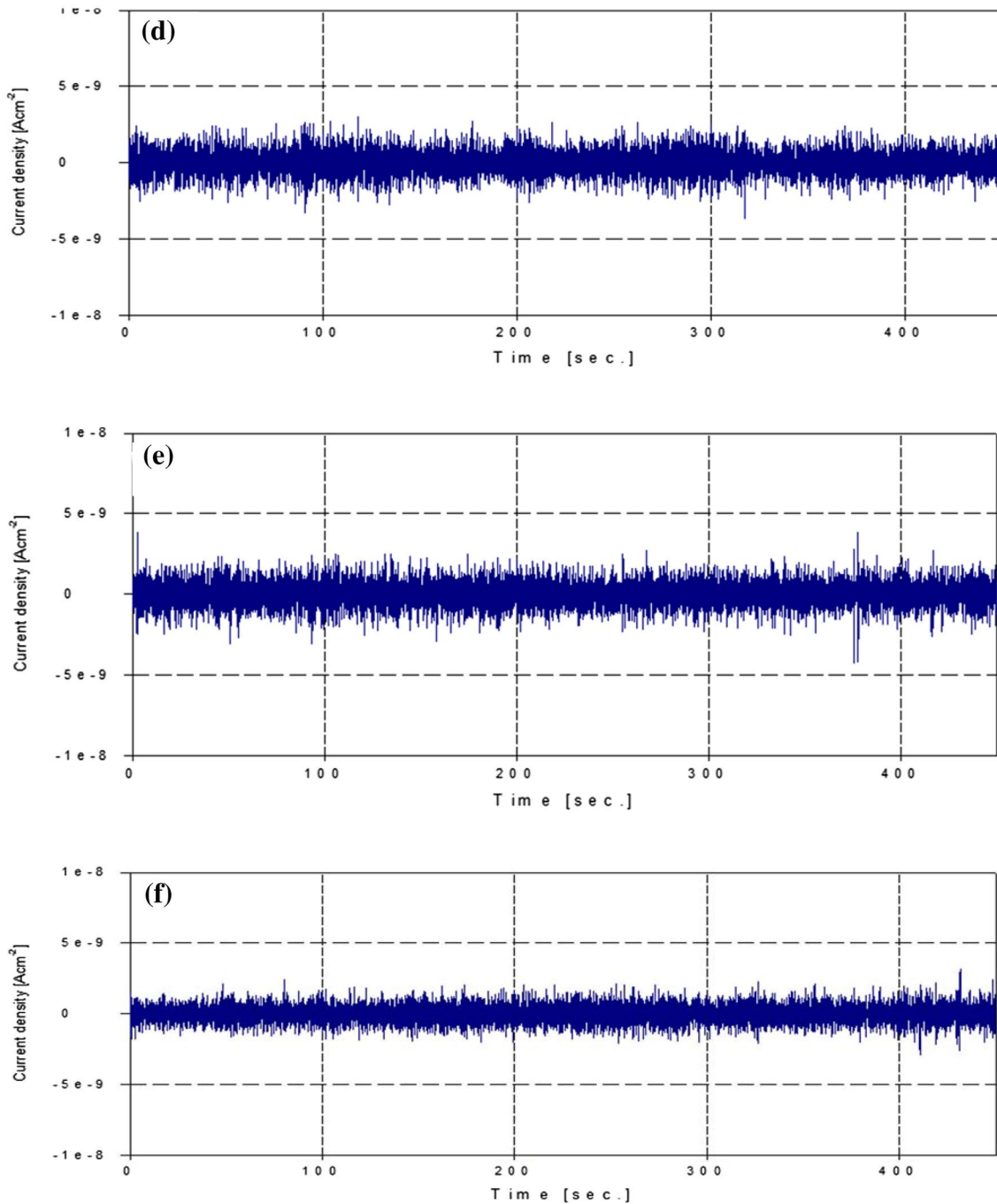


Fig. 11 (continued)

$$V_{i,\text{noise}} = V_i - V_{i,\text{DC}} \tag{7}$$

A similar procedure can be applied to calculate  $I_{i,\text{noise}}$ . Figure 10 demonstrates an example of DC drift removal of current data. Figure 10a shows the DC current before trend removal, and Fig. 10b shows both the DC trend and the noise data using MAR method with  $p = 64$ . Extracted real current

and voltage data noise were investigated in the time domain to calculate the noise resistance  $R_n$ .

Figure 11 demonstrates the electrochemical current noise of AA2024 immersed in 3.5% NaCl solution with different concentrations of *ELUS*. It can be observed that the amplitude of current noise (represents the activity of corrosion process) shows a strong correlation with increasing inhibitor concentration where it sharply decreases with the increase

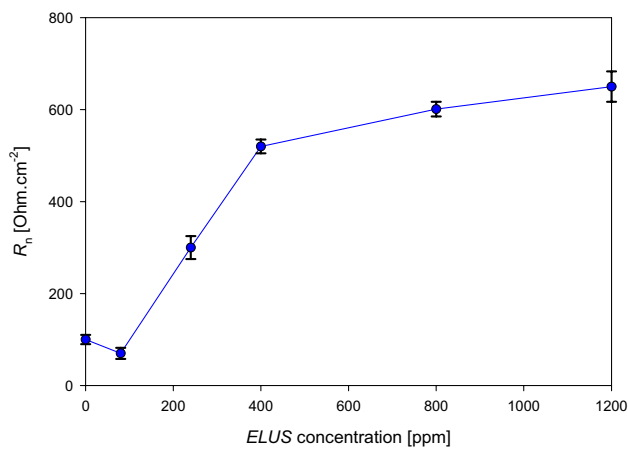


**Fig. 12** Change of noise resistance ( $R_n$ ) of AA2024 with the concentration of *ELUS* inhibitor in 3.5% NaCl

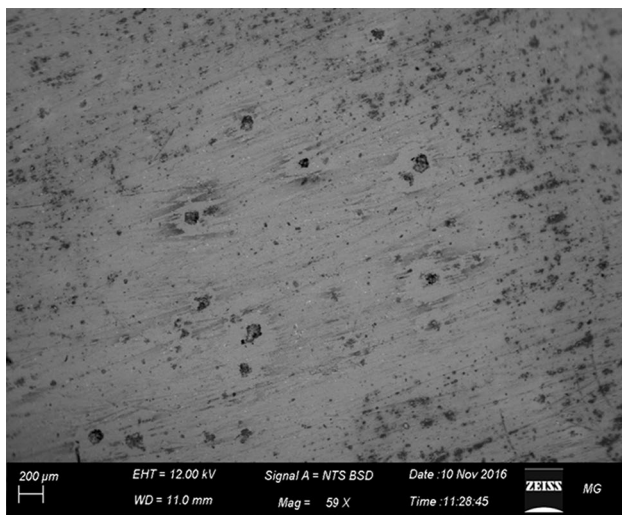


**Fig. 13** SEM images of aluminum after immersion in 3.5% NaCl solution for 24 h in the absence of *ELUS*

in the inhibitor concentration (with exception of 80 ppm). Moreover, the frequency of fluctuations of the current noise, which represents the frequency of events (i.e., pitting), also decreases with the increase in the inhibitor concentration [29]. The continuous decrease in current noise seems to be related to improving the film formed on the metal surface due to adsorption of inhibitor.

The height of fluctuations of the blank sample appears to be less than that of 80 ppm of *ELUS*; however, the frequency of fluctuation of the blank sample is greater than that of 80 ppm *ELUS*. These results indicate that the blank sample experiences a uniform corrosion with a slight pitting than that of 80 ppm of *ELUS*. Moreover, by increasing the inhibitor concentration more than 80 ppm, both the frequency of noise and noise height gradually decrease indicating inhibition of

corrosion process. These results are in line with both EIS and PDP results.

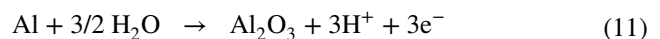
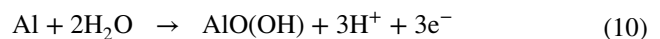
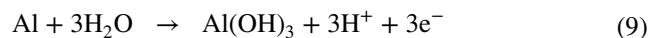
The noise resistance ( $R_n$ ) of AA2024 in 3.5% NaCl solution with a different concentration of *ELUS* is presented in Fig. 12. The figure demonstrates a continuous increase in  $R_n$  with *ELUS* concentration except for 80 ppm case. Besides, the  $R_n$  values are comparable to that of  $R_{ct}$  that calculated from EIS data fitting. These results will be confirmed by studying the surface morphology of both blank and 1200 ppm *ELUS* samples in the next section.

Generally, the aluminum oxide layer cannot protect the surface from corrosion in severe corrosive environments such as 3.5% NaCl. In such corrosive media, AA2024 undergoes pitting corrosion. The pitting of aluminum is mainly due to its low negative potential and the presence of  $\text{Cl}^-$ . The mechanism of the pitting corrosion of Al in neutral NaCl medium includes reduction of oxygen as a cathodic reaction as follows:



The alkalinity would increase due to the production of hydroxide group. The presence of weak fatty acids may decrease the effect of this alkalinity.

The anodic reactions that take place in this neutral solution are assumed as one of the following reactions [8–10]:



This follows the formation of  $\text{Al}(\text{OH})^{+2}$  which will react with chloride ion to form a soluble complex as follows:



The concentration of  $\text{Cl}^-$  increases the production of the soluble complex ions ( $\text{Al}(\text{OH})\text{Cl}^+$ ) and consequently magnifies the corrosion rate of aluminum [31]. In addition, the presence of the intermetallic particles, mainly  $\text{Al}_2\text{MgCu}$  which cover 3% of the aluminum alloy surface, plays an important role in the corrosion process. The intermetallic particles form cathodic sites with respect to the aluminum matrix, and this change in the electrochemical activities of alloy composition forms micro-galvanic cells leading to pitting corrosion [32].

The above corrosion mechanism of aluminum can be inhibited by means of depositing a barrier layer that hinders the diffusion of electrolyte toward the aluminum surface and/or formation of an insoluble salt over the aluminum surface. This can be achieved by adsorption of an organic inhibitor such as the *ELUS*. Also, the water sparingly soluble fatty acid (extract content) can replace the  $\text{Cl}^-$  during interaction with aluminum hydroxide.



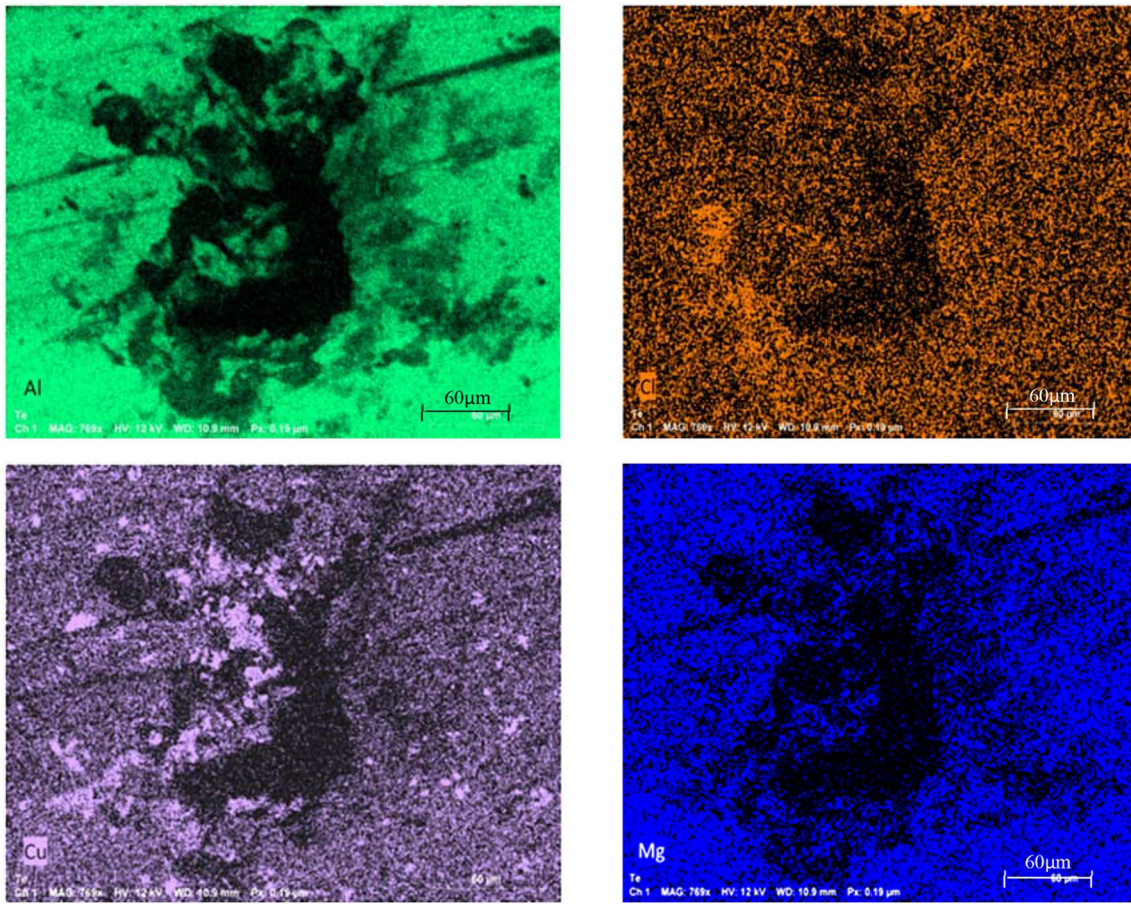


**Fig. 14** EDX mapping of AA2024 sample after immersion for 24 h in 3.5% NaCl solution in the absence of *ELUS*

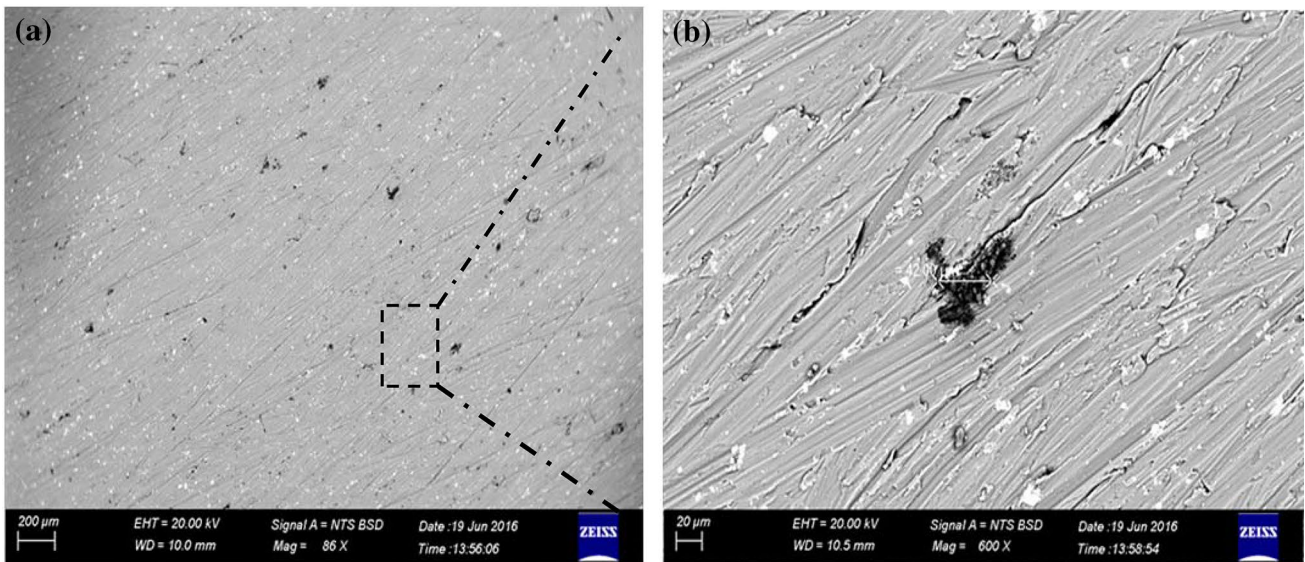


**Fig. 15** SEM images of aluminum after immersion in 3.5% NaCl solution for 24 h: (a) in the presence of inhibitor 1200 ppm *LU* and (b) in the presence of inhibitor (magnified)

#### 4 Scanning Electron Microscopy (SEM)

Through the use of SEM, we were able to investigate in detail the surface morphology of different samples. SEM analysis was conducted for both bare and inhibited samples. The SEM image (Fig. 13) displays AA2024 surface after immersion in 3.5% NaCl for 24 h with no *ELUS* inhibitor. Severe pitting corrosion can be clearly observed covering the whole sample surface. The EDX elemental mappings analysis of a selected pit within the surface is presented in Fig. 14. It is clear from the elemental maps that corrosion products within the pit are mainly aluminum chloride. In addition, copper and magnesium, representing the intermetallic particles, appeared within the pit. These intermetallic particles have different potential than that of aluminum matrix initiating pitting corrosion. These results have further strengthened our confidence in the mechanism of corrosion suggested above.

The surface morphology of inhabited sample was also studied using SEM technique. The SEM images, as shown in Fig. 15, show the surface of AA2024 sample with 1200 ppm *ELUS* after 24 h of immersed in 3.5% NaCl. Neither corrosion products nor pitting can be observed from SEM images. It can be concluded that the presence of *ELUS* suppressed the corrosion process due to the formation of an adsorbed film of *ELUS* on the surface of AA2024. This film prohibits or hinders the oxygen reduction reaction on the metal surface and therefore protects AA2024 from pitting and uniform corrosions in 3.5% NaCl solution. Finally, the results of SEM analysis are consistent with previous electrochemical results.

#### 5 Conclusions

A new green inhibitor was extracted from of *L. Usitatis-simum* (*ELUS*) seeds and used to inhibit the corrosion of AA2024 in artificial seawater. The kinetics of corrosion inhibition are based on the results obtained from the polarization study, EIS, EN measurements and morphology study (optical and SEM). The efficiency of corrosion inhibition increased with increasing the inhibitor (*ELUS*) concentration. Polarization study reveals that *ELUS* acts as a cathodic-type inhibitor. According to EIS results, the charge transfer resistance governed the corrosion process. The results of *EN* measurements showed that *ELUS* provides protection against pitting corrosion of aluminum in the presence of chloride ions. The *EN* results are confirmed by SEM and EDX analysis. *EN* results are compatible with the measurements of potentiodynamic and *EIS*. The inhibition action was achieved via adsorption of the *ELUS* compounds on the surface of AA2024.

**Acknowledgements** The authors would also like to thank Bassem Zaghloul, Military Technical College, Cairo, Egypt, for their invaluable advices during this work. Moreover, the authors would like to thank Zeiss SEM team in Cairo, Egypt, for their invaluable advice during conducting SEM.

#### References

- Rajasekar A, Xiao W, Sethuraman M, Parthipan P, Elumalai P (2017) Airborne bacteria associated with corrosion of mild steel 1010 and aluminum alloy 1100. *Environ Sci Pollut Res* 24:8120–8136
- Akid R, Gobara M, Wang H (2011) Corrosion protection performance of novel hybrid polyaniline/sol–gel coatings on an aluminium 2024 alloy in neutral, alkaline and acidic solutions. *Electrochim Acta* 56:2483–2492
- Rahsepar M, Mohebbi F, Hayatdavoudi H (2017) Synthesis and characterization of inhibitor-loaded silica nanospheres for active corrosion protection of carbon steel substrate. *J Alloy Compd* 709:519–530
- Umoren SA, Eduok UM (2016) Application of carbohydrate polymers as corrosion inhibitors for metal substrates in different media: a review. *Carbohydr Polym* 140:314–341
- Ameh PO, Eddy NO (2013) Commiphora pedunculata gum as a green inhibitor for the corrosion of aluminium alloy in 0.1 M HCl. *Res Chem Intermed* 40:2641–2649
- Akin M, Nalbantoglu S, Cuhadar O, Uzun D, Saki N (2015) Juglans regia L. extract as green inhibitor for stainless steel and aluminium in acidic media. *Res Chem Intermed* 41:899–912
- Wang YG, Chen Y, Zhao YW, Zhao D, Zhong YA, Qi F et al (2017) A reinforced organic-inorganic layer generated on surface of aluminium alloy by hybrid inhibitors. *J Mol Liq* 225:510–516
- Khadraoui A, Khelifa A, Hachama K, Mehdaoui R (2016) Thymus algeriensis extract as a new eco-friendly corrosion inhibitor for 2024 aluminium alloy in 1 M HCl medium. *J Mol Liq* 214:293–297
- Winkler DA, Breedon M, White P, Hughes AE, Sapper ED, Cole I (2016) Using high throughput experimental data and in silico models to discover alternatives to toxic chromate corrosion inhibitors. *Corros Sci* 106:229–235
- Umoren SA, Obot IB, Ebenso EE, Okafor PC, Ogbobe O, Oguzie EE (2006) Gum arabic as a potential corrosion inhibitor for aluminium in alkaline medium and its adsorption characteristics. *Anti-Corros Methods Mater* 53:277–282
- Obot I, Obi-Egbedi N, Umoren S (2009) Antifungal drugs as corrosion inhibitors for aluminium in 0.1 M HCl. *Corros Sci* 51:1868–1875
- Zadeh ARH, Danaee I, Maddahy MH (2013) Thermodynamic and adsorption behaviour of medicinal nitramine as a corrosion inhibitor for AISI steel alloy in HCl solution. *J Mater Sci Technol* 29:884–892
- Ménager M, Azémard C, Vieillescazes C (2014) Study of Egyptian mummification balms by FT-IR spectroscopy and GC–MS. *Microchem J* 114:32–41
- Jackson M, Mantsch HH (1995) The use and misuse of FTIR spectroscopy in the determination of protein structure. *Crit Rev Biochem Mol Biol* 30:95–120
- Pawlak A, Mucha M (2003) Thermogravimetric and FTIR studies of chitosan blends. *Thermochim Acta* 396:153–166
- Li L, Qu Q, Bai W, Yang F, Chen Y, Zhang S et al (2012) Sodium diethyldithiocarbamate as a corrosion inhibitor of cold rolled steel in 0.5 M hydrochloric acid solution. *Corros Sci* 59:249–257

17. Gupta NK, Verma C, Quraishi M, Mukherjee A (2016) Schiff's bases derived from L-lysine and aromatic aldehydes as green corrosion inhibitors for mild steel: experimental and theoretical studies. *J Mol Liq* 215:47–57
18. Grassino AN, Halambek J, Djaković S, Rimac Brnčić S, Dent M, Grabarić Z (2016) Utilization of tomato peel waste from canning factory as a potential source for pectin production and application as tin corrosion inhibitor. *Food Hydrocoll* 52:265–274
19. Roberge PR (2000) Handbook of corrosion engineering. McGraw-Hill, New York
20. Fontana MG (2005) Corrosion engineering. Tata McGraw-Hill Education, New York
21. Hassan HH, Abdelghani E, Amin MA (2007) Inhibition of mild steel corrosion in hydrochloric acid solution by triazole derivatives: part I. Polarization and EIS studies. *Electrochimica Acta* 52:6359–6366
22. Solmaz R, Kardaş G, Culha M, Yazıcı B, Erbil M (2008) Investigation of adsorption and inhibitive effect of 2-mercaptothiazoline on corrosion of mild steel in hydrochloric acid media. *Electrochim Acta* 53:5941–5952
23. Gobara M, Zaghoul B, Baraka A, Elsayed M, Zorainy M, Kotb MM et al (2017) Green corrosion inhibition of mild steel to aqueous sulfuric acid by the extract of *Corchorus olitorius* stems. *Mater Res Express* 4:046504
24. Ibrahim T, Habbab M (2011) Corrosion inhibition of mild steel in 2 M HCl using aqueous extract of eggplant peel. *Int J Electrochem Sci* 6:5357–5371
25. Yang L (2008) Techniques for corrosion monitoring. Elsevier, Amsterdam
26. Le Thu Q, Bierwagen G, Touzain S (2001) EIS and ENM measurements for three different organic coatings on aluminum. *Prog Org Coat* 42:179–187
27. Koh E, Park S (2017) Self-anticorrosion performance efficiency of renewable dimer-acid-based polyol microcapsules containing corrosion inhibitors with two triazole groups. *Prog Org Coat* 109:61–69
28. Markhali B, Naderi R, Mahdavian M, Sayebani M, Arman S (2013) Electrochemical impedance spectroscopy and electrochemical noise measurements as tools to evaluate corrosion inhibition of azole compounds on stainless steel in acidic media. *Corros Sci* 75:269–279
29. Tan Y (2009) Sensing localised corrosion by means of electrochemical noise detection and analysis. *Sens Actuators B Chem* 139:688–698
30. Ashassi-Sorkhabi H, Seifzadeh D, Hosseini M (2008) EN, EIS and polarization studies to evaluate the inhibition effect of 3H-phenothiazin-3-one, 7-dimethylamin on mild steel corrosion in 1 M HCl solution. *Corros Sci* 50:3363–3370
31. Obayes HR, Al-Amiery AA, Alwan GH, Abdullah TA, Kadhum AAH, Mohamad AB (2017) Sulphonamides as corrosion inhibitor: experimental and DFT studies. *J Mol Struct* 1138:27–34
32. Buchheit R, Grant R, McKenzie B, Zender G (1997) Local dissolution phenomena associated with S phase ( $Al_2CuMg$ ) particles in aluminum alloy 2024T3. *J Electrochem Soc* 144:2621